Spinodal decomposition to control magnetotransport in (Ge,Mn) films

I.-S. Yu,[1,2,3] M. Jamet,[1] T. Devillers,[1] A. Barski,[1] P. Bayle-Guillemaud,[1] C. Beigné,[1] J. Rothman,[4] V. Baltz,[5] and J. Cibert[2]
[1]*Institut des Nanosciences et Cryogénie, SP2M, CEA-UJF, F-38054 Grenoble, France*
[2]*Institut Néel, CNRS-UJF, BP 166, F-38042 Grenoble, France*
[3]*Graduate Institute of Electronics Engineering, National Taiwan University, Taipei, 10617 Taiwan, Republic of China*
[4]*Laboratoire d'Electronique et des Technologies de l'Information, CEA, F-38054 Grenoble, France*
[5]*Institut des Nanosciences et Cryogénie, Spintec, CEA-CNRS-UJF-INPG, F-38054 Grenoble, France*
(Received 3 May 2010; revised manuscript received 22 June 2010; published 16 July 2010)

Changing the morphology of the growing surface and the nature of residual impurities in (Ge,Mn) layers dramatically changes nanospinodal decomposition, i.e., the morphology of ferromagnetic Mn-rich inclusions. By this way, we are able to control the magnetotransport properties of (Ge,Mn) films. By using different substrates and substrate preparation, we have indeed obtained *p*-type layers with nanocolumns, either parallel or entangled, and *n*-type layers with spherical clusters. Holes exhibit an anomalous Hall effect and electrons exhibit a tunneling magnetoresistance, both with a clear dependence on the magnetization of the Mn-rich inclusions; holes exhibit orbital MR and electrons show only the normal Hall effect, and an additional component of magnetoresistance due to weak localization, all three being independent of the magnetic state of the Mn-rich inclusions. Identified mechanisms point to the position of the Fermi level of the Mn-rich material with respect to the valence band of germanium as a crucial parameter for the control and the optimization of magnetotransport in such hybrid layers.

DOI: 10.1103/PhysRevB.82.035308 PACS number(s): 75.50.Pp, 61.46.−w, 75.47.−m, 75.75.−c

I. INTRODUCTION

Research on ferromagnetic semiconductors triggered enormous activity due to their potential use in spintronics.[1,2] Up to now, efforts have mainly focused on diluted magnetic semiconductors (DMSs) in which magnetic atoms randomly substitute the host matrix atoms.[3] Their magnetic properties can be manipulated by electric fields making them suitable materials for spintronic applications provided that they can be made ferromagnetic above room temperature. However, well-controlled DMSs based on II-VI and III-V semiconductors still exhibit very low values of the Curie temperature T_C.

Many groups have reported T_C values well above room temperature in semiconductors doped with magnetic transition metals (TMs), along with remarkable magnetotransport and magneto-optical properties. Although the observation of such properties has been often taken to support an intrinsic origin of ferromagnetism in a DMS, it is now admitted that such a behavior may be attributed to TM-rich areas resulting from nanospinodal decomposition.[4] Such features have been theoretically predicted[5] and reported in (Ge,Mn),[6–10] and in Cr and Fe-doped GaN (Refs. 11 and 12) or ZnTe.[13] In this field of intense materials research, goals are now (i) controlling nanospinodal decomposition to reproducibly stabilize high-T_C TM-rich areas and tailor desirable magnetic properties, and (ii) enhancing the coupling with carriers to give rise to strong magnetoresistance (MR) or anomalous Hall effect (AHE).

In this paper, we demonstrate the fine control of nanospinodal decomposition and magnetotransport in (Ge,Mn) films grown on Ge and GaAs(001) substrates. We focus on (Ge,Mn) because it is compatible with mainstream silicon technology, and nanospinodal decomposition leads to high-T_C values in layers grown on Ge substrate. Growing (Ge,Mn) films on GaAs(001) semi-insulating ($\rho > 10^7$ Ω cm) substrates makes in-plane transport measurements easier and constitutes a first step toward spin injection from (Ge,Mn) into a GaAs-based spin-light-emitting diode.[14] Using different preparations of the GaAs surface promotes the diffusion of Ga or As into the (Ge,Mn) layer. We describe the influence of these electrically active impurities, and of the morphology of the surface, on the nanocolumn growth, on one hand, and on the electrical properties, on the other hand. We thus address the major issue of the influence of codoping (either *n* or *p* type) on nanospinodal decomposition in group IV magnetic semiconductors, demonstrating a strong influence on the shape of the Mn-rich precipitates. We also provide hints to control and optimize magnetotransport properties of the (Ge,Mn) films. We show that magnetization-dependent AHE and MR are not optimized simultaneously, and we propose a general picture based on the electrical doping of the matrix and on the position of Fermi level in the precipitates with respect to the valence band of Ge.

II. EXPERIMENTS

(Ge,Mn) films were grown by low-temperature molecular-beam epitaxy (MBE), using growth conditions as described in Refs. 6 and 9. Samples grown on Ge substrates, labeled Ge-(Ge,Mn) in the following, constitute our reference samples. In the present study, the substrate temperature was $T_g = 100$ °C and deposition rate ~0.2 Å s^{-1}. This corresponds to the regime of "low growth temperature" of Ref. 9, which minimizes the formation of Ge_3Mn_5 clusters. In the case of GaAs substrates, we have used two different methods to prepare the initial surface. In the first one, the native oxide was thermally desorbed from an *epiready* substrate, by raising the substrate temperature up to almost 600 °C. The (Ge,Mn) layers was grown directly on the resulting Ga-rich

 ©2010 The American Physical Society

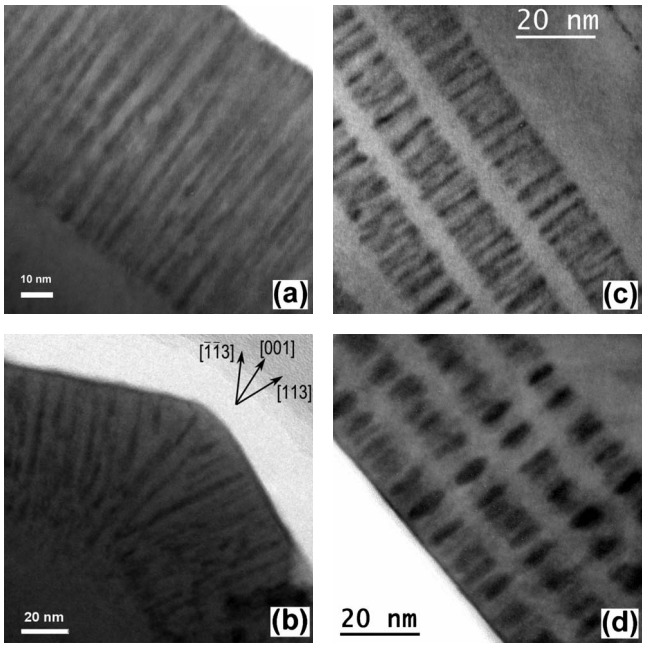

FIG. 1. TEM cross section of (Ge,Mn) films grown on Ge(001). (a) 80-nm-thick $Ge_{0.9}Mn_{0.1}$ film grown at 100 °C according to the surface preparation described in Ref. 9. (b) $Ge_{0.94}Mn_{0.06}$ film grown at 100 °C on the facetted Ge surface. (c) and (d) $(GeMn/Ge)_4$ superlattices grown on Ge. The Ge spacer is 5 nm thick. The Mn concentration, deposition rate, and growth temperature are 6%, 0.2 Å/s, and 100 °C in (c) and 10%, 0.13 Å/s, and 140 °C in (d), respectively.

GaAs surface, which was rough as observed by reflection high-energy electron diffraction. Such samples will be labeled Ga-(Ge,Mn). In the second case, As-(Ge,Mn) samples, a thin undoped GaAs buffer layer was grown first in a separate III-V system, protected with an amorphous As capping, and transferred in air to the IV-IV MBE machine. Desorbing the As capping layer at 200 °C results in an atomically flat, (2×4) reconstructed, As-rich surface. Magnetization was measured using a superconducting quantum interference device (SQUID). Magnetotransport properties (MR and Hall effect) were investigated using Hall bars defined by optical lithography, aligned along a ⟨110⟩ direction, of width 20 μm, with voltage probes separated by 140 μm. Transmission electron microscopy (TEM) observations were performed using a JEOL 4000EX microscope with an acceleration voltage of 400 kV.

III. FILM MORPHOLOGY

In Ge-(Ge,Mn) films, a typical morphology is that of long parallel Mn-rich nanocolumns,[6] growing normal to the Ge(001) substrate surface as shown in Fig. 1(a). On a Ge buffer layer grown on a Ge(001) substrate with {113} facets obtained by anisotropic chemical etching in an H_2O_2 aqueous solution [Fig. 1(b)], they grow perpendicular to the facets. This general picture fully agrees with two-dimensional (2D) nanospinodal decomposition, driven by surface diffusion and aggregation of Mn atoms, with nucleation of Mn-rich areas taking place during the first stage of the growth.[5] As a consequence of this mechanism, the columns are always perpendicular to the growing surface. We could further demonstrate that Mn atoms only diffuse within the topmost atomic layers by growing $(GeMn/Ge)_4$ superlattices [Figs. 1(c) and 1(d)]. Indeed (Ge,Mn) layers containing Mn-rich nanocolumns are well separated by 5-nm-thick pure Ge spacers showing that the diffusion of Mn atoms along the growth direction is only weakly activated. Moreover, by increasing the growth temperature and Mn content to obtain larger columns[9] and decreasing the growth rate to favor Mn surface diffusion, we could find a clear vertical self-organization of nanocolumns [Fig. 1(d)]. If we assume that the lattice parameters within the columns and the Ge matrix are different, larger columns lead to an enhanced residual strain field which favors the nucleation of nanocolumns on top of each other as in quantum dots superlattices.[15]

In Ga-(Ge,Mn) films also, we observe nanocolumns, but they are bent according to the initial surface roughness [Figs. 2(a) and 2(b)], and this results in a highly disordered pattern. However, after depositing a 40-nm-thick Ge buffer layer to flatten the initial GaAs(001) surface [Figs. 2(c) and 2(d)], nanocolumns are parallel to each other and well aligned along the [001] growth direction. This is again in agreement with 2D nanospinodal decomposition. Note that a secondary ion mass spectroscopy (SIMS) analysis of such Ga-(Ge,Mn) films confirms the outdiffusion of Ga, which is an acceptor in germanium, from the GaAs(001) substrate into the (Ge,Mn) film [inset in Fig. 4(a)].

By contrast [Figs. 2(e) and 2(f)], the As-(Ge,Mn) layers feature randomly distributed Mn-rich precipitates. The same random distribution of nanoclusters is observed when increasing the nominal Mn content from 2% to 6% and 10% at $T_g=100$ °C, but for an increase in the average precipitate density and length along the growth direction. This suggests that the decomposition is of three-dimensional (3D) character and mostly driven by nucleation. In addition, a few Ge_3Mn_5 clusters already start to form, as evidenced by their typical Moiré contrast [see inset of Fig. 3(d)]. SIMS measurements shown in the inset of Fig. 5(b), performed on the As-(Ge,Mn) samples, evidences an As-rich topmost layer extending over 3 ± 1 nm (as given by the plateau in the SIMS profile) below the sample surface and containing up to almost 3×10^{19} As cm^{-3}, i.e., an integrated amount of approximately one monolayer As. This is a consequence of the segregation of As atoms, initially present at the GaAs surface, during the growth of Ge, with a well-known surfactant effect.[16] Accordingly, as described below, the As-(Ge,Mn) films appear as *n* doped: As atoms are shallow donors in Ge, and in this topmost layer they compensate *p*-type doping by substitutional Mn. The presence of As near the surface of the growing layer offers a possible explanation for this change of character of the nanospinodal decomposition, from 2D to 3D. According to Ref. 17, Mn atoms are incorporated into germanium in a subsurface interstitial position and further diffuse within the growth plane: this offers a mechanism for 2D nanospinodal decomposition.[5] Codoping with As changes the charge state of Mn atoms, thus reducing Coulomb repulsion and enhancing the effect of attractive Mn-Mn pair interaction, making the nucleation of Mn-rich precipitates easier.[4]

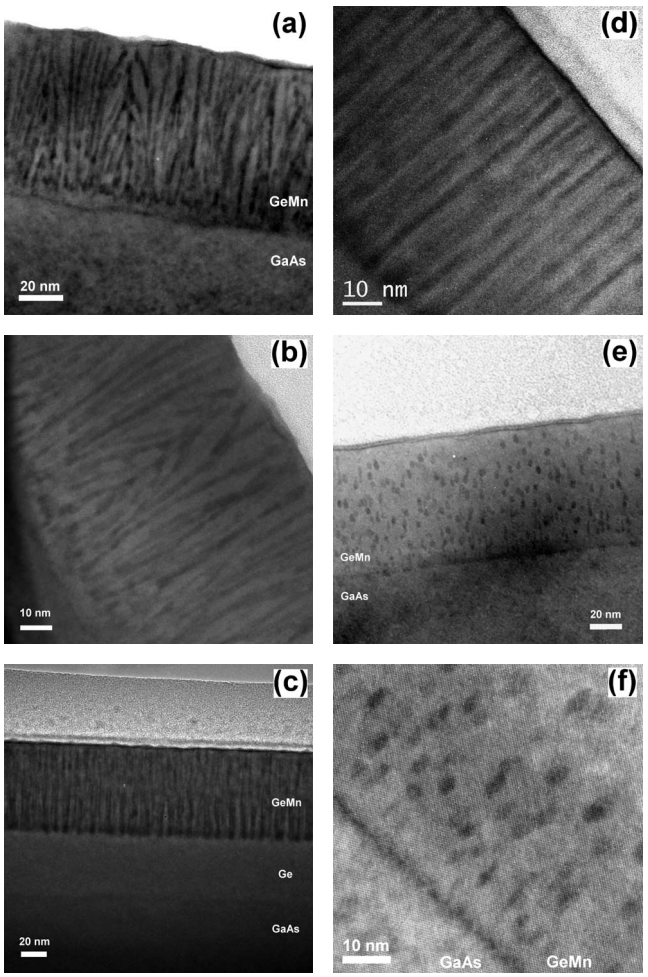

FIG. 2. TEM cross section of 80-nm-thick layers grown at 100 °C: (a) low magnification and (b) high magnification Ga-$Ge_{0.9}Mn_{0.1}$ film, (c) low magnification and (d) high magnification $Ge_{0.94}Mn_{0.06}$ film after depositing a 40-nm-thick Ge buffer on GaAs(001), and (e) low magnification and (f) high magnification As-$Ge_{0.98}Mn_{0.02}$ film.

In addition to that mechanism, the presence of donors like As is expected to displace the equilibrium between interstitial Mn (another donor) and substitutional Mn (an acceptor), enhancing the amount of substitutional Mn (which form nucleation centers for further Mn aggregation[18]) and reducing the amount of interstitial Mn (thus decreasing the incorporation into already existing clusters). Finally, the presence of a large amount of As atoms on the growth front may influence the decomposition kinetics by drastically reducing the surface diffusion of Mn atoms and favoring random nucleation. These different mechanisms induced by the presence of As conspire to favor a growth process dominated by nucleation, contributing to make the nanospinodal decomposition 3D.

IV. MAGNETIC PROPERTIES

As shown in Fig. 3, all samples contain several magnetic phases: two in the case of Ga-(Ge,Mn) [Figs. 3(a) and 3(b)] or three in the case of As-(Ge,Mn) [Figs. 3(c) and 3(d)]. More precisely they exhibit (i) a strong paramagnetic signal with a $1/T$ temperature dependence at low temperature, attributed to Mn atoms diluted in the Ge matrix, and well fitted using a 3/2-Brillouin function;[19] (ii) a contribution attributed to the superparamagnetic Mn-rich nanocolumns or precipitates, with finite T_C and blocking temperature T_B; and (iii) in As-(Ge,Mn) only (in agreement with the TEM observation), a contribution from Ge_3Mn_5 clusters with a broad range of blocking temperatures.

In the Ga-(Ge,Mn) sample shown in the inset of Fig. 3(a), we have first assumed that the magnetization of ferromagnetic nanocolumns saturates below 5 T (see Ref. 9) which is the maximum field we could apply in the SQUID. Then we subtracted a 3/2-Brillouin function from paramagnetic Mn atoms to the sample magnetization curve in order to obtain the saturating magnetic signal from the columns at 5 K. By this method, we could estimate that 60 ± 6 % of the magnetic moments are in the matrix and 40 ± 6 % are in nanocolumns, with $T_C \approx 150$ K, $T_B = 15 \pm 5$ K [Fig. 3(b)], and $(1.0 \pm 0.1)\mu_B$/Mn. The average magnetic moment of a nanocolumn is $(520 \pm 50)\mu_B$ as given by Langevin fits shown in Fig. 3(a).

For the As-(Ge,Mn) sample in Fig. 3(c), as discussed before, we have subtracted a 3/2-Brillouin function to the sample magnetization curve in order to obtain the saturating magnetic signal at 5 K. However, in this sample, both Mn-rich precipitates and Ge_3Mn_5 clusters contribute to this signal. The Curie temperature of Mn-rich precipitates is $T_C \approx 50$ K [Fig. 3(d)]; thus, the magnetic signal at 100 K only originates from Ge_3Mn_5 clusters and the difference between the saturating signals at 5 and 100 K gives the contribution from Mn-rich precipitates. We finally found that 52 ± 3 % of the magnetic moments are in the matrix, 22 ± 2 % in Mn-rich precipitates with $T_C \approx 50$ K, $T_B = 15 \pm 5$ K [Fig. 3(d)] and $(1.2 \pm 0.2)\mu_B$/Mn, and 26 ± 2 % in Ge_3Mn_5 clusters. After subtracting the magnetic contributions from diluted Mn and Ge_3Mn_5 clusters at 30 K, we could fit the magnetization curve with a Langevin function and find the average magnetic moment per precipitate to be $(100 \pm 20)\mu_B$.

V. MAGNETOTRANSPORT

From the slope of the Hall effect measured at high field (not shown), both Ge-(Ge,Mn) and Ga-$Ge_{0.9}Mn_{0.1}$ films are p type. Actually Mn was reported as a double acceptor in germanium, with acceptor levels 160 and 370 meV above the valence-band edge,[20] respectively: for such a deep acceptor, the Mott critical density is expected to be well in the 10^{20} cm^{-3} range. In Ge-(Ge,Mn), due to a strong AHE, the Hall slope can be used only to give a lower bound to the hole density, which is at least in the high 10^{19} cm^{-3} range, and we observe a metallic behavior, suggesting doping above the Mott density. In Ga-$Ge_{0.9}Mn_{0.1}$, the AHE is weaker [see Fig. 4(c)], so that the apparent density deduced from the Hall effect, up to 3×10^{19} cm^{-3} at 300 K, is meaningful. It is clear in this case that the presence of holes is not due solely to the Mn acceptors: for a measured density one order of magnitude lower than the Mott density we should observe a strongly activated conductivity,[21] while we observe [Fig.

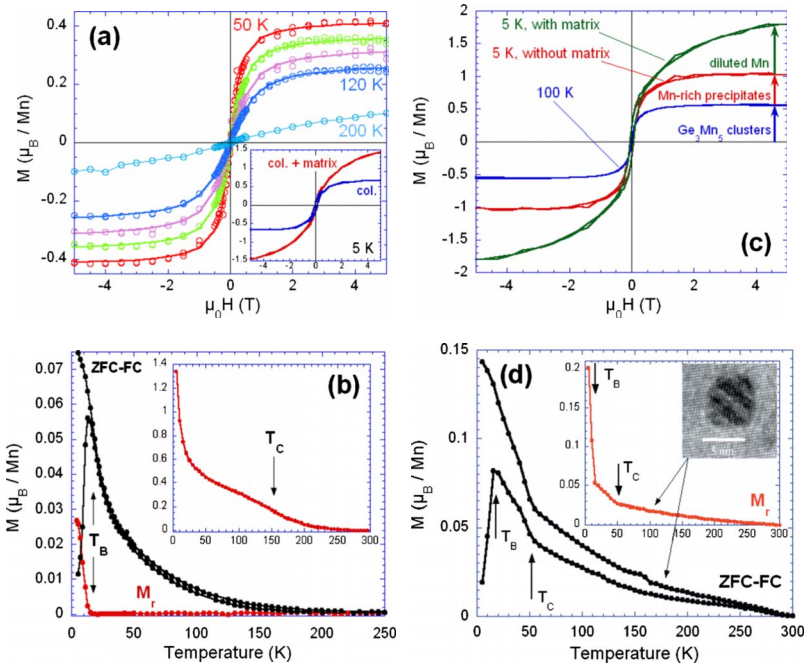

FIG. 3. (Color online) Magnetic measurements performed on (a) and (b) Ga-$Ge_{0.9}Mn_{0.1}$ and (c) and (d) As-$Ge_{0.94}Mn_{0.06}$ samples, respectively. (a) Magnetization curves recorded at different temperatures. Open circles are experimental data and solid lines are fits using a Langevin function for $T=50$, 80, 100, and 120 K. At 200 K, nanocolumns are paramagnetic. The inset shows magnetization curves at 5 K with and without the paramagnetic contribution from diluted Mn atoms in the Ge matrix. (b) Zero field cooled–field cooled (ZFC-FC) curves at 0.015 T and magnetic remanence M_r after maximum field cooling at 5 T. Inset: saturation magnetization at 2 T. (c) Magnetization curves recorded at 5 and 100 K showing the respective contributions from diluted Mn, Mn-rich precipitates, and Ge_3Mn_5 clusters. (d) ZFC-FC curves at 0.015 T and magnetic remanence M_r after maximum field cooling at 5 T. Inset: TEM image of a Ge_3Mn_5 cluster.

4(a)] a weak temperature dependence. This can be explained by the presence of Ga, as revealed by SIMS, since Ga is a shallow acceptor in germanium (11 meV). However, we note also that if the Fermi level of the Mn-rich metallic material forming the precipitates lies below the top of the valence band in germanium, then no Schottky barrier, and even an accumulation layer, is formed around each precipitate [see the inset in Fig. 4(c)]. We then expect a weak—if any—temperature dependence of the apparent carrier density. We expect also the buildup of an electric field pattern pointing toward each nanocolumn. Then the magnetotransport properties can be understood as follows: (i) as the nanocolumns configuration is well below the percolation threshold, holes have to propagate through the germanium matrix; that makes the basis of the conductivity; (ii) however, the electric field pattern drags the holes through the nanocolumns, where the conductivity is higher; applying a magnetic field suppresses this effect, creating the geometrically enhanced orbital MR (OMR), or extraordinary MR (EMR),[22] which we observed to be strong in Ge-(Ge,Mn) (Ref. 6); (iii) finally, the absence of Schottky barrier enhances the interaction of holes with Mn atoms in the nanocolumns, thus allowing a spin polarization and AHE to appear.[6] Moreover we could recently show by means of finite element simulations that AHE and the carrier mobility in the Ge matrix are key parameters for EMR.[23] Indeed, we found that EMR increases when increasing the

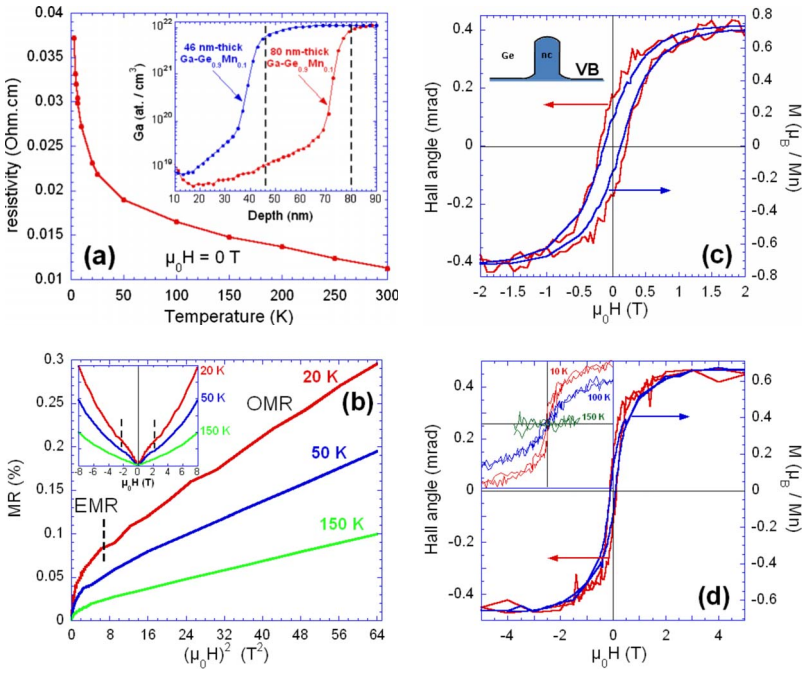

FIG. 4. (Color online) Magnetotransport in Ga-$Ge_{0.9}Mn_{0.1}$; the magnetic field is applied normal to the film plane: (a) temperature dependence of the zero-field resistivity. Inset: SIMS measurements performed on two Ga-$Ge_{0.9}Mn_{0.1}$ films of different thicknesses and showing reproducible Ga outdiffusion into the (Ge,Mn) film; (b) MR (in %) up to 8 T as a function of $(\mu_0 H)^2$ and recorded at 20, 50, and 150 K. Two separate MR contributions can be identified: EMR at low magnetic field and OMR at high field. Inset: MR (in %) as a function of $\mu_0 H$. (c) and (d) AHE (red curve) compared to magnetization (blue curve) at 2–3 and 4–5 K, respectively. Inset: AHE at 10, 100, and 150 K.

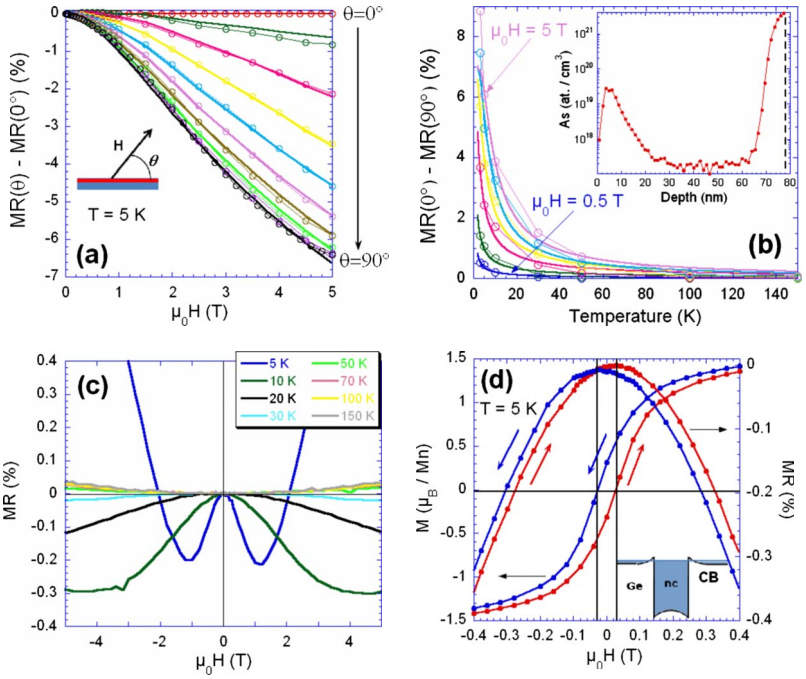

FIG. 5. (Color online) Magnetotransport in As-$Ge_{0.94}Mn_{0.06}$. (a) Field dependence and (b) temperature dependence of the MR anisotropy, for different orientations of the field; symbols are experimental data, solid lines are calculated ones. The inset in (b) shows the SIMS profile of As atoms. (c) and (d) MR and magnetization as functions of the field applied in plane. In (d), the field sweep directions are indicated by colored arrows attached to the plots.

carrier mobility and AHE. In Ga-(Ge,Mn) samples, we still observe positive MR as shown in Fig. 4(b), with the same temperature dependence as in Ref. 6, but much weaker. The dependence of MR on $(\mu_0 H)^2$ exhibits two separate contributions: a linear dependence at high field corresponding to OMR as a consequence of the Ge valence-band degeneracy and EMR at low field. EMR exhibits a V shape and linear dependence on $\mu_0 H$ [inset in Fig. 4(b)]. Its very low value is readily explained by considering the dependence of EMR on the carrier mobility. Due to the higher disorder and induced defects, the carrier mobility in Ga-(Ge,Mn) sample is lower than in Ge-(Ge,Mn) by more than one order of magnitude which leads to EMR by orders of magnitude lower as experimentally observed. EMR further vanishes with AHE above $T_C \approx 150$ K and only OMR remains. Finally, at very low temperature, negative MR is observed (not shown) which is due to (i) isotropic giant magnetoresistance (GMR) on the Mn-rich nanocolumns[23] although the spin diffusion length of holes is very short due to spin-orbit coupling and (ii) spin disorder scattering[24] on Mn atoms diluted in the Ge matrix as typical in metallic DMS. These effects are weak and rapidly lost when raising the temperature. AHE in Ga-(Ge,Mn) nicely matches the magnetization of the nanocolumns [Figs. 4(c) and 4(d)]. Again, the effect is weaker than in Ge-(Ge,Mn) by almost two orders of magnitude. This is expected from the lower mobility: it was pointed out in Ref. 25 that scattering on impurities such as Ga atoms [SIMS measurements in the inset of Fig. 4(a) have indeed shown that Ga outdiffused from the GaAs substrate] partly suppresses the effect of skew scattering.

As-(Ge,Mn) films exhibit metallic *n*-type conductivity as already observed by Tsuchida *et al.*[26] This is clearly due to the presence of As donors in the topmost layer. Hence, magnetotransport essentially measures the properties of this 3-nm-thick layer. We observe no AHE, as expected since spin-orbit scattering is small for electrons in the conduction band of germanium, and also because the same assumptions as above (Fermi level of metallic Mn-rich precipitates lying below the top of the valence band) suggest that a high Schottky barrier is formed for electrons [see the inset in Fig. 5(d)]. At low temperature, the overall magnetoresistance is negative and reaches −7.5% under 9 T at 5 K. Strong negative magnetoresistance (called colossal magnetoresistance) is observed in doped manganite perovskites as a consequence of magnetic-field-driven ferromagnetic-to-paramagnetic phase transition.[27] However, in our case we show that negative magnetoresistance is due to quantum effects (weak localization) and tunneling magnetoresistance (TMR). MR first exhibits a highly anisotropic part [Fig. 5(a)]: we show now that this is due to 2D weak localization in the As-doped layer, which vanishes when the field is applied in plane ($\theta = 0$). Weak localization and anisotropic magnetoresistance were also observed in degenerate *p*-$Ge_{1-x}Mn_xTe$ ($x \geq 0.1$) by Fukuma *et al.*[28] and Lim *et al.*,[29] respectively. The low-field isotropic part [Figs. 5(c) and 5(d)] will be analyzed later on in terms of tunneling magnetoresistance between Mn-rich precipitates in agreement with the granular nature of As-(Ge,Mn) films. The MR of noninteracting electrons in the 2D weak localization regime is $\Delta\rho/\rho \approx -\Delta\sigma/\sigma = -A f_2[4e\mu_0 H \sin(\theta) L_\phi/\hbar]$,[30] where $A = e^2/2\pi^2\hbar\sigma_{2D}(0)$, L_ϕ is the phase relaxation length, and the function $f_2(x)$ is defined in Ref. 30. Fits in Fig. 5(a) were obtained with only two adjustable parameters: A and L_ϕ. We used $A = 4\%$, close to the value $A = 6 \pm 2$ % calculated using the experimental value of the 2D conductivity at $H = 0$. We used $L_\phi = 11.5$ nm large enough with respect to the thickness of the conducting layer to justify the use of the 2D regime of weak localization. In the above expression, we have neglected spin-orbit scattering: the spin-orbit time is much longer than the electron phase relaxation time: $\tau_{SO} \gg \tau_\phi$. This assumption relies on the fact that intrinsic spin-orbit coupling of conduction electrons is weak in germanium due to crystal inversion symme-

try, making spin-dependent scattering like Diakonov-Perel mechanism inefficient. Moreover the exchange coupling between electrons and paramagnetic diluted Mn atoms is very weak, and the phase coherence length is less than the average distance between Mn-rich precipitates limiting electron spin scattering on them. In angular fits of MR, we have also made the assumption that the intervalley scattering time is very short (much shorter than τ_ϕ) and thus we neglected the diffusion coefficient anisotropy (i.e., the anisotropy of L_ϕ) due to nonspherical Fermi surfaces in germanium. Finally, fits of the temperature dependence of the anisotropic MR [Fig. 5(b)] were obtained by simply writing $L_\phi = \sqrt{D\tau_\phi}$, using the temperature dependence of the diffusion coefficient D for an n-doped degenerate semiconductor[31] and a temperature dependence of the phase relaxation time $\tau_\phi \propto T^{-\alpha}$, with $\alpha \approx 1.7$, similar to those obtained in Ref. 32 for Ge:Sb ($\alpha = 1.5$) and in Ref. 33 for Si-metal-oxide-semiconductor field-effect transistors ($\alpha = 1.6$), and currently attributed to both electron-electron and electron-phonon collisions. Turning back to the isotropic MR, [Figs. 5(c) and 5(d)], it contains a negative contribution, which features two maxima at the coercive field of Mn-rich precipitates, and vanishes above 50 K as does their magnetization. Hence, we tentatively ascribe it to TMR through the precipitates and the Schottky barriers formed around them. By analogy with spin injection from a ferromagnetic metal to a semiconductor,[34] efficient spin injection from the precipitate to the matrix requires an interface resistance, provided by the Schottky barrier. This barrier must be high enough to prevent full spin relaxation inside the precipitate but reasonably transparent to allow tunnel MR to occur.

VI. CONCLUSION

To summarize, we have shown that codoping has a major influence on nanospinodal decomposition in (Ge,Mn) films and on the magnetotransport properties. For films grown on GaAs substrates with a Ga-rich surface, we recovered 2D nanospinodal decomposition, as in layers grown on germanium substrates, with nanocolumns perpendicular to the growing surface. Electrical properties are similar to what we obtained on Ge(001) substrates except that the presence of defects in the films leads to weaker positive MR and AHE; GMR is also observed at very low temperature. For films grown on As-rich flat surfaces, 3D nanospinodal decomposition is observed due to As codoping and magnetotransport is dominated by TMR and weak localization, while AHE is negligible. These results are consistent with the assumption that the Fermi level of the Mn-rich metallic precipitates lies in front of the valence band of the Ge matrix.

ACKNOWLEDGMENTS

The authors would like to thank A. Arnoult (LAAS, Toulouse) for providing As-capped GaAs substrates, and T. Dietl and J. Pernot for fruitful discussions. This work was granted by the Agence Nationale pour la Recherche (project GeMO) and the Nanoscience Foundation in Grenoble (project IMAGE).

[1] A. H. MacDonald, P. Schiffer, and N. Samarth, Nature Mater. **4**, 195 (2005).
[2] T. Dietl, Semicond. Sci. Technol. **17**, 377 (2002).
[3] H. Ohno, Science **281**, 951 (1998).
[4] T. Dietl, J. Appl. Phys. **103**, 07D111 (2008).
[5] K. Sato, H. Katayama-Yoshida, and P. H. Dederichs, Jpn. J. Appl. Phys., Part 2 **44**, L948 (2005).
[6] M. Jamet, A. Barski, T. Devillers, V. Poydenot, R. Dujardin, P. Bayle-Guillemaud, J. Rothman, E. Bellet-Amalric, A. Marty, J. Cibert, R. Mattana, and S. Tatarenko, Nature Mater. **5**, 653 (2006).
[7] D. Bougeard, S. Ahlers, A. Trampert, N. Sircar, and G. Abstreiter, Phys. Rev. Lett. **97**, 237202 (2006).
[8] A. P. Li *et al.*, Phys. Rev. B **75**, 201201(R) (2007).
[9] T. Devillers, M. Jamet, A. Barski, V. Poydenot, P. Bayle-Guillemaud, E. Bellet-Amalric, S. Chérifi, and J. Cibert, Phys. Rev. B **76**, 205306 (2007).
[10] D. Bougeard, N. Sircar, S. Ahlers, V. Lang, G. Abstreiter, A. Trampert, J. M. Lebeau, S. Stemmer, D. W. Saxey, and A. Cerezo, Nano Lett. **9**, 3743 (2009).
[11] L. Gu, S. Y. Wu, H. X. Liu, R. K. Singh, N. Newman, and D. J. Smith, J. Magn. Magn. Mater. **290-291**, 1395 (2005).
[12] A. Bonanni, A. Navarro-Quezada, Tian Li, M. Wegscheider, Z. Matej, V. Holy, R. T. Lechner, G. Bauer, M. Rovezzi, F. D'Acapito, M. Kiecana, M. Sawicki, and T. Dietl, Phys. Rev. Lett. **101**, 135502 (2008).
[13] S. Kuroda, N. Nishizawa, M. Mitome, Y. Bando, K. Osuch, and T. Dietl, Nature Mater. **6**, 440 (2007).
[14] R. Fiederling, M. Keim, G. Reuscher, W. Ossau, G. Schmidt, A. Waag, and L. W. Molenkamp, Nature (London) **402**, 787 (1999).
[15] J. Tersoff, C. Teichert, and M. G. Lagally, Phys. Rev. Lett. **76**, 1675 (1996).
[16] A. Leycuras, Appl. Phys. Lett. **66**, 1800 (1995).
[17] W. G. Zhu, H. H. Weitering, E. G. Wang, E. Kaxiras, and Z. Y. Zhang, Phys. Rev. Lett. **93**, 126102 (2004).
[18] W. Zhu, Z. Zhang, and E. Kaxiras, Phys. Rev. Lett. **100**, 027205 (2008).
[19] T. C. Schulthess and W. H. Butler, J. Appl. Phys. **89**, 7021 (2001).
[20] H. H. Woodbury and W. W. Tyler, Phys. Rev. **100**, 659 (1955).
[21] P. Achatz, J. Pernot, C. Marcenat, J. Kacmarcik, G. Ferro, and E. Bustarret, Appl. Phys. Lett. **92**, 072103 (2008).
[22] S. A. Solin, T. Thio, D. R. Hines, and J. J. Heremans, Science **289**, 1530 (2000).
[23] I.-S. Yu, M. Jamet, T. Devillers, A. Barski, P. Bayle-Guillemaud, C. Beigné, J. Rothman, V. Baltz, and J. Cibert (unpublished).
[24] F. Matsukura, H. Ohno, A. Shen, and Y. Sugawara, Phys. Rev. B **57**, R2037 (1998).
[25] Y. D. Park, A. T. Hanbicki, S. C. Erwin, C. S. Hellberg, J. M.

Sullivan, J. E. Mattson, T. F. Ambrose, A. Wilson, G. Spanos, and B. T. Jonker, Science **295**, 651 (2002).
[26] R. Tsuchida, J. T. Asubar, Y. Jinbo, and N. Uchitomi, J. Cryst. Growth **311**, 937 (2009).
[27] A. P. Ramirez, J. Phys.: Condens. Matter **9**, 8171 (1997).
[28] Y. Fukuma, K. Goto, S. Senba, S. Miyawaki, H. Asada, T. Koyanagi, and H. Sato, J. Appl. Phys. **103**, 053904 (2008).
[29] S. T. Lim, J. F. Bi, K. L. Teo, Y. P. Feng, T. Liew, and T. C. Chong, Appl. Phys. Lett. **95**, 072510 (2009).
[30] B. L. Altshuler and A. G. Aronov, in *Electron-Electron Interactions in Disordered Systems*, edited by A. L. Efros and M. Pollak (North-Holland, Amsterdam, 1985), p. 1.
[31] S. M. Sze, *Physics of Semiconductors Devices* (Wiley, New York, 1981).
[32] T. A. Polyanskaya and I. I. Saidashev, JETP Lett. **34**, 361 (1981).
[33] M. J. Uren, R. A. Davies, M. Kaveh, and M. Pepper, J. Phys. C **14**, L395 (1981).
[34] A. Fert and H. Jaffrès, Phys. Rev. B **64**, 184420 (2001).